

<https://helda.helsinki.fi>

Conversion of ALD CuO Thin Films into Transparent Conductive p-Type CuI Thin Films

Weiss, Alexander

2023-01

Weiss , A , Goldmann , J , Kettunen , A S , Popov , G , Iivonen , T , Mattinen , M , Jalkanen , P , Hatanpää , T , Leskelä , M , Ritala , M & Kemell , M 2023 , ' Conversion of ALD CuO Thin Films into Transparent Conductive p-Type CuI Thin Films ' , Advanced Materials Interfaces , vol. 10 , no. 3 , 2201860 . <https://doi.org/10.1002/admi.202201860>

<http://hdl.handle.net/10138/356052>

<https://doi.org/10.1002/admi.202201860>

cc_by

publishedVersion

Downloaded from Helda, University of Helsinki institutional repository.

This is an electronic reprint of the original article.

This reprint may differ from the original in pagination and typographic detail.

Please cite the original version.

Conversion of ALD CuO Thin Films into Transparent Conductive p-Type CuI Thin Films

Alexander Weiß, Jacqueline Goldmann, Sakari Kettunen, Georgi Popov, Tomi Iivonen, Miika Mattinen, Pasi Jalkanen, Timo Hatanpää, Markku Leskelä, Mikko Ritala, and Marianna Kemell*


Copper iodide (CuI) is a high-performance p-type transparent semiconductor that can be used in numerous applications, such as transistors, diodes, and solar cells. However, the lack of conformal and scalable methods to deposit CuI thin films limits its establishment in applications that involve complex-shaped and/or large substrate areas. In this work, atomic layer deposition (ALD) is employed to enable scalable and conformal thin film deposition. A two-step approach relying on ALD of CuO and its subsequent conversion to CuI via exposure to HI vapor at room temperature is demonstrated. The resulting CuI films are phase-pure, uniform, and of high purity. Furthermore, CuI films on several substrates such as Si, amorphous Al₂O₃, n-type TiO₂, and γ -CsPbI₃ perovskite are prepared. With the resulting n-TiO₂/p-CuI structure, the easy and straightforward fabrication of a diode structure as a proof-of-concept device is demonstrated. Moreover, the successful deposition of CuI on γ -CsPbI₃ proves the compatibility of the process for using CuI as the hole transport layer in perovskite solar cell applications in the nip-configuration. It is believed that the ALD-based approach described in this work will offer a viable alternative for depositing transparent conductive p-type CuI thin films in applications that involve complex high aspect ratio structures and large substrate areas.

1. Introduction

The search for high-performance transparent p-type conductors has been a major challenge for the development of transparent

A. Weiß, J. Goldmann, S. Kettunen, G. Popov, T. Iivonen, M. Mattinen, T. Hatanpää, M. Leskelä, M. Ritala, M. Kemell
Department of Chemistry
University of Helsinki
P. O. Box 55, Helsinki FI-00014, Finland
E-mail: marianna.kemell@helsinki.fi

P. Jalkanen
Department of Physics
University of Helsinki
P. O. Box 43, Helsinki FI-00014, Finland

 The ORCID identification number(s) for the author(s) of this article can be found under <https://doi.org/10.1002/admi.202201860>.

© 2022 The Authors. Advanced Materials Interfaces published by Wiley-VCH GmbH. This is an open access article under the terms of the Creative Commons Attribution License, which permits use, distribution and reproduction in any medium, provided the original work is properly cited.

DOI: 10.1002/admi.202201860

electronics for decades. One of the most promising candidates to resolve this issue is copper(I) iodide (CuI) thanks to its high optical transparency in the visible spectral range.^[1] CuI has a wide direct bandgap (3.1 eV)^[2,3] and typically shows p-type semiconductivity due to its copper vacancies. These provide an outstanding hole mobility (44 cm² V⁻¹ s⁻¹).^[4] Therefore, the performance of CuI surpasses other, oxide-based p-type semiconductors.^[5] Tuning of the stoichiometry enables a wide range of carrier concentrations (10¹⁶ to 10²⁰ cm⁻³) and allows to control the p-type conductivity (maximum: 283 S cm⁻¹).^[3,6] These superior electrical properties of CuI are based on two reasons: First, the electronegativity of iodine is smaller than that of oxygen, introducing an acceptor state with more delocalized holes above the valence band maximum.^[5] Second, the large I⁻ radius (220 pm) and the three outermost p-orbitals provide sufficient orbital overlap for fast hole transport.^[3] As an additional asset, CuI consists

of abundant, nontoxic, and low-cost elements. For these reasons, CuI has been reported for numerous applications such as transparent conductors,^[7] thermoelectric devices,^[8–10] heterojunction diodes,^[5,11–15] thin-film transistors,^[16–20] and solar cells.^[21–25]

Out of these applications, in particular the young research field of perovskite solar cells (PSCs) has become highly promising in the past decade due to its potential to deliver low-cost solar energy using abundant materials.^[26] PSCs recently reached a power conversion efficiency (PCE) of 25.5%^[27,28] which is close to the PCE of conventional Si-based solar cells. PSC structures consist of a halide perovskite (e.g., CH₃NH₃PbI₃, CsPbI₃, CsSnI₃) as the light harvesting layer, which is sandwiched between a n-type electron transport layer (ETL) (e.g., n-TiO₂) and a p-type hole transport layer (HTL) (e.g., p-CuI).^[29,30] However, for PSCs to become widely commercially available requires thin film deposition methods which are scalable to large substrate areas and preferably complex-shaped surfaces.^[31–34]

We believe to overcome this challenge by employing atomic layer deposition (ALD). ALD has enabled many industrial applications, such as electroluminescent displays^[35] and

microelectronics.^[36] Reason for that is its excellent capability to deposit uniform and conformal thin films.^[37–40] Although ALD is considered to be rather slow and expensive compared to other thin film deposition techniques, its inherent scalability to large areas and batches, or alternatively to roll-to-roll processing,^[41,42] enables high throughput which outbalances its slowness. The highest reported throughput is 10 000 silicon solar cells per hour being encapsulated and passivated with ALD Al₂O₃.^[43]

Although CuI has been reported to be grown by numerous thin film deposition methods at low temperatures,^[3,44,45] currently ALD lacks processes to deposit CuI. The library for ALD processes^[46] is vast and to date exhibits more than 1400 processes for over 500 compounds. However, the field of ALD metal halides is yet largely unexplored. In particular, for metal iodides only three processes exist so far—two for PbI₂^[47,48] and the one for CsI^[49] that we developed recently.

Developing an ALD process for CuI was challenging. As a first approach, we tried to apply similar chemistry as what has been used for ALD of metal fluorides. These processes typically rely on β -diketonates as metal precursors and volatile metal fluorides as halide precursors. We used copper(II) acetylacetonate (Cu(acac)₂) or bis(2,2,6,6-tetramethyl-3,5-heptanedionato) copper(II) (Cu(thd)₂) as the copper precursors and titanium(IV) iodide (TiI₄) as the iodine precursor. However, these precursor combinations yielded only particle deposits rather than continuous films. Furthermore, the growth per cycle (GPC) ≤ 0.04 Å per cycle of these processes were extremely low. Therefore, we outreached for a different approach to make CuI thin films by ALD.

The solid–gas reaction approach that we reported previously^[50] to convert PbO₂ films into PbI₂ films by exposure to hydroiodic acid (HI) vapor gave us new motivation. We hypothesized that the exposure of an ALD CuO thin film^[51] to HI vapor would trigger a similar conversion reaction, resulting in a CuI thin film. Although this approach would include a second, non-ALD step, it could still maintain the advantages of ALD to make thin films for scalable and conformal applications, such as for PSCs. As an additional asset, the low deposition temperature of the underlying CuO ALD process would make it compatible with various substrates, such as perovskites in a nip-junction.

We herein report a new conversion pathway to form CuI thin films from ALD CuO thin films and HI vapor. The CuO thin films were prepared according to literature^[51] from bis(dimethylamino-2-propoxy) copper(II) (Cu(dmap)₂) as the copper precursor and ozone as the oxygen precursor. The conversion of these films was performed at room temperature in a reduced pressure glass reactor by exposure to HI vapor. The demonstrated pathway is fast, simple, and straightforward and yields phase pure, uniform, and high purity CuI thin films. Owing to the low deposition temperature (80–140 °C) used in the underlying CuO ALD process, we demonstrate formation of CuI thin films on various substrates: silicon, sapphire, amorphous Al₂O₃, and γ -CsPbI₃ perovskite. We used n-type TiO₂ as a substrate and formed a pn-junction to fabricate a diode structure as proof-of-concept device. Moreover, for the application of CuI as the HTL in the nip-configuration PSCs, we successfully deposited CuI on γ -CsPbI₃ perovskite to demonstrate the compatibility of this process with a halide perovskite as a substrate.

2. Results and Discussion

2.1. Film Deposition

We deposited ALD CuO thin films on silicon, Al₂O₃ and TiO₂ substrates using the optimized parameters given in literature^[51] and varying the number of deposition cycles (Figure 1a). We found different GPC values on these substrates, the one on Si being 0.30 Å per cycle which is in excellent agreement with the literature value. On Al₂O₃ and TiO₂, we observed slightly lower GPCs of 0.25 and 0.19 Å per cycle, respectively.

Conversions of the ALD CuO thin films were performed at room temperature in a small glass reactor containing a glass boat filled with 200 μ L of hydroiodic acid (HI) (for detailed experimental setup, see Figure S1, Supporting Information). The conversion of CuO to CuI starts immediately upon reducing the pressure in the reaction chamber and is fast and straightforward. The glass reactor allowed us to visually observe the progress of the conversion reaction (Video S1, Supporting Information). The visual appearance of the films changed

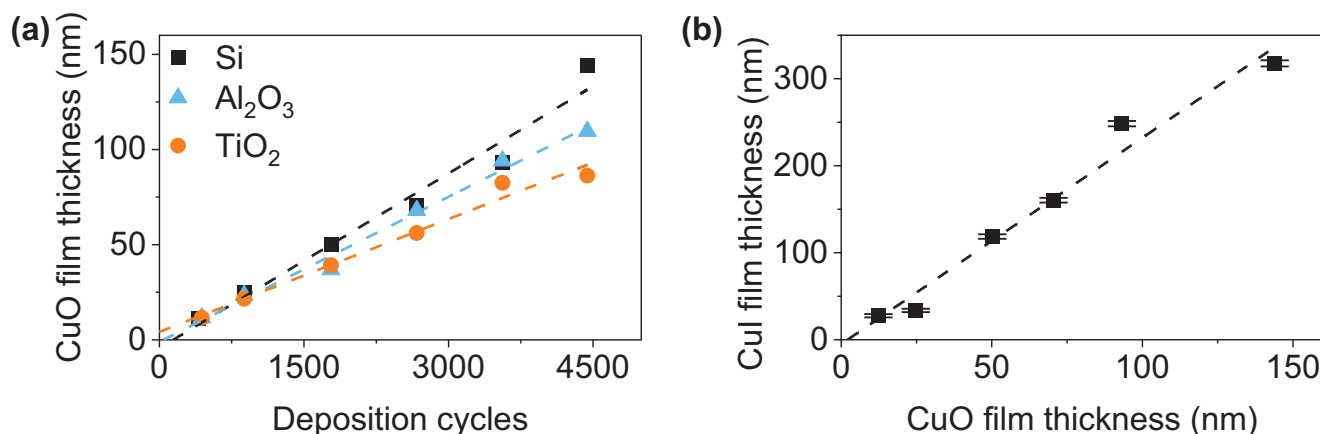


Figure 1. a) CuO film thickness on Si, Al₂O₃, and TiO₂ substrates as a function of the number of deposition cycles, deposited at 120 °C with pulse durations of 2.0 s for both Cu(dmap)₂ and O₃, and 2.0 s purge durations. b) Thicknesses of the converted CuI films as a function of the initial CuO film thicknesses on Si.

during the conversion due to changes in the bandgap, thickness and roughness of the film, which translate into changes in the reflectance and transmittance. Therefore, completion of the conversion is indicated by the lack of further changes in the film appearance. The reaction front advances from the edges of the CuO film toward its center. We saw no changes in the film color after 60 s, but to ensure full conversion, we exposed the CuO films to the HI vapor for 5 min.

The converted CuI film thicknesses differed strongly from the initial ALD CuO film thicknesses. We observed in average a 2.4-fold thickness increase upon conversion on all substrates (Figure 1b, for information on other substrates see Figure S2, Supporting Information). This can be traced back to the larger sum of ionic radii of Cu^+ and I^- (3.0 Å) compared to that of Cu^{2+} and O^{2-} (2.1 Å) and the consequent molar volume difference of CuI (33.6 $\text{cm}^3 \text{mol}^{-1}$) compared to that of CuO (12.6 $\text{cm}^3 \text{mol}^{-1}$).

We faced challenges when converting very thin or thick ALD CuO films to CuI on different substrates. With thin initial CuO films (<25 nm thickness), we observed pinholes in the converted CuI films on soda lime glass, Al_2O_3 and TiO_2 substrates (Figures S3 and S4, Supporting Information). On Si, CuI films were pinhole-free from initial CuO thicknesses ≥ 50 nm (Figure S3, Supporting Information). Changes in temperature (<0 °C), pressure or HI concentration still yielded phase-pure CuI, but did not show any minimizing effect on the number of pinholes in the converted films (Figure S5, Supporting Information). Another challenge occurred upon

conversion of thick CuO films (>100 nm thickness). Some of these films spontaneously burst and peeled off of the substrate upon conversion (Video S2, Supporting Information). We observed the same behavior on other substrates (TiO_2 and amorphous Al_2O_3), too, when the initial CuO film thickness exceeded 100 nm. That is why we suspect the strong thickness increase mentioned previously to result in a critical stress in the converted CuI films which can cause them to burst off of the substrate. For these reasons, we conclude that this process works well with initial CuO films in a thickness range between 25–100 nm.

2.2. Film Properties

X-ray diffraction (XRD) measurements confirmed the phase-purity of all ALD deposited CuO and converted CuI thin films (Figure 2a,b). We deposited CuO films at several temperatures (80–140 °C) and verified the desired monoclinic tenorite^[52] phase in the whole temperature range. After the conversion, we were able to assign all the reflections to the γ -CuI phase without traces of residual crystalline CuO.

Evaluation by top-down field-emission scanning electron microscopy (FESEM) showed that both the ALD CuO and the converted CuI thin films were continuous, uniform and pinhole-free. It also revealed that the grains of the CuI thin films are much larger compared to the initial ALD CuO grains

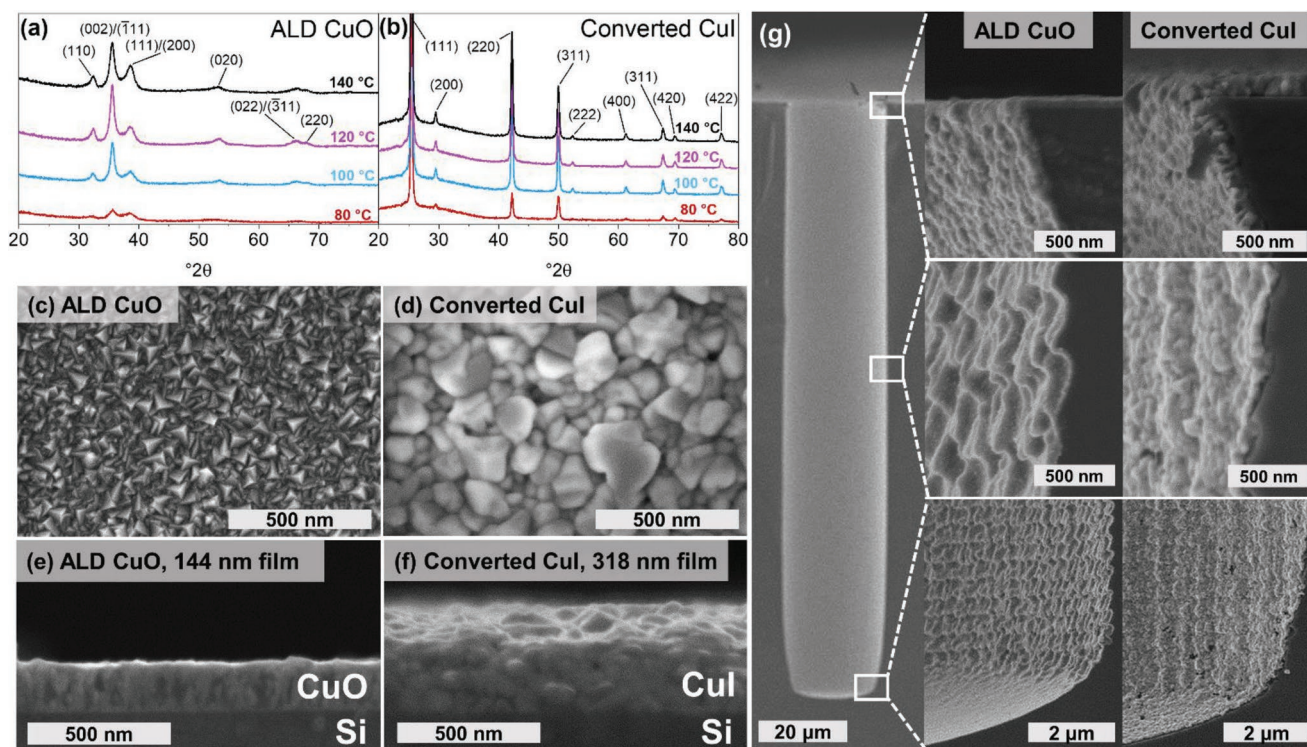


Figure 2. GIXRD patterns of a) ALD CuO films deposited on Si at different temperatures and b) the corresponding converted CuI thin films. Top-down FESEM images of c) a CuO thin film deposited on Si with 4440 cycles at 120 °C and d) the corresponding converted CuI film. Cross-sectional FESEM images of e) a ALD CuO thin film deposited on Si with 4440 cycles at 120 °C and f) the corresponding converted CuI film. g) Cross-sectional FESEM image of a hole with 6:1 AR in a patterned Si substrate. CuO was deposited first, followed by conversion to CuI. ALD CuO was deposited at 120 °C with 2140 cycles.

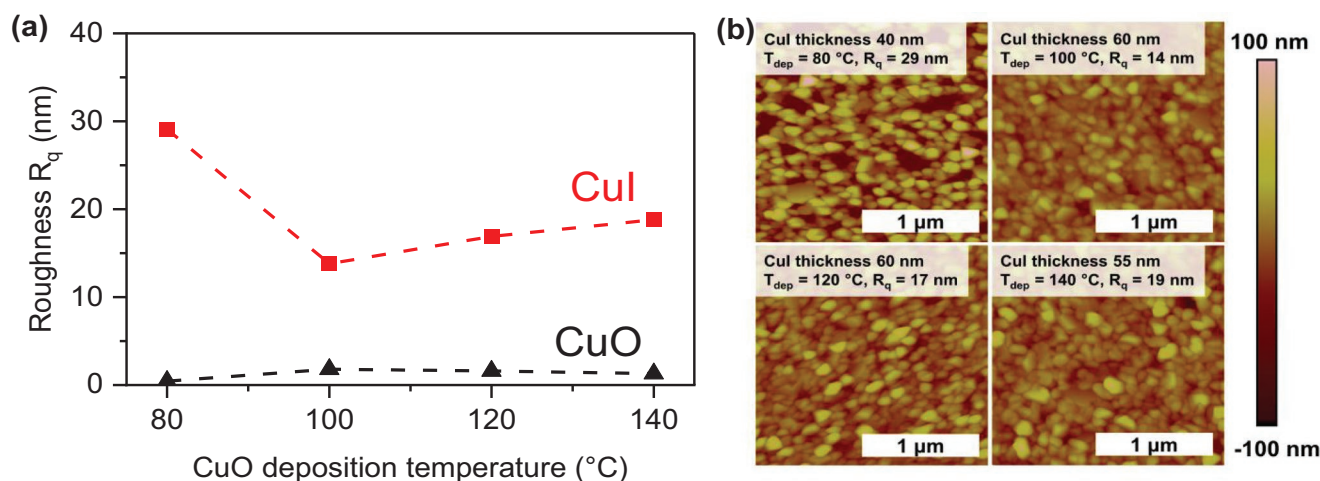


Figure 3. a) AFM roughness R_q as a function of the CuO deposition temperature. b) AFM images of CuI films after the conversion from ALD CuO films deposited at different temperatures. CuO films were deposited with 1000 cycles.

(Figure 2c,d). Cross-sectional FESEM images (Figure 2e,f) confirm the significant thickness increase upon conversion, which is in agreement with our previously mentioned findings (Figure 1b). The conformality advantage of ALD is retained in our approach for making CuI films from ALD CuO films. Without any process parameter optimizations, we were able to deposit a CuO film with good conformality in holes with 6:1 aspect ratio (AR) and successfully convert it to CuI (Figure 2g).

The surface roughnesses R_q of the CuI films measured by atomic force microscopy (AFM) increased significantly compared to the initial CuO surface roughness (Figure 3a). We measured R_q values from films deposited at different temperatures (80–140 °C). While the ALD CuO process deposited smooth films ($R_q < 2$ nm) in the whole temperature range, we saw the appearance of pinholes after the conversion of films deposited at 80 °C, causing a drastic increase in the CuI surface roughness. These findings were consistent with the previously mentioned observations: pinholes occurred only in CuI films converted from thin CuO films with < 25 nm in thickness (Figure 3b). As evident from literature,^[51] CuO films grown at lower deposition temperatures with the same number of cycles are thinner due to their smaller GPC. In comparison, CuI films made from CuO films deposited at 100 °C and above showed much smoother surfaces thanks to the lack of pinholes. The R_q gradually increased toward the higher end of the temperature range due to grains growing larger.

Characterization of film compositions with ToF-ERDA before and after the conversion showed that the films were stoichiometric CuO and CuI, respectively (Table 1). The Cu to O ratio for the CuO, as well as the Cu to I ratio for the CuI were close to 1:1. There was only a small amount (< 2 at%) of light element impurities in both films. Most notably, oxygen was detected in CuI, which made us to suspect whether the conversions were complete. However, as evident from the ToF-ERDA depth profiles, we were able to assign the oxygen to the native SiO₂ layer on the Si substrate (Figure S6, Supporting Information). Therefore, the remarkably low O impurity level in the converted CuI films highlights the facility and completeness of this film preparation pathway.

We found the optical properties of both the ALD CuO and converted CuI films to be in good agreement with those reported in literature. The ALD CuO films appear brownish-dark and absorb in the visible range (Figure 4a), whereas the converted CuI films are transparent in the visible range and absorb in the UV range (Figure 4b). We attribute these absorptions to the bandgap absorptions of both materials. The bandgaps determined from the respective Tauc plots^[53,54] (Figure 4 insets) for CuO (indirect, 1.1 eV, lit.: 1.0–1.4 eV)^[55] and CuI (direct, 3.0 eV, lit.: 3.1 eV)^[2] were in excellent agreement with the literature values.

Electrical properties of the ALD CuO and converted CuI thin films were determined via 4-point-probe sheet resistance measurements from films deposited at different temperatures (80–140 °C) (Figure 5a). The CuO thin films showed typical^[51] resistivities (20–300 Ω cm), whereas the CuI films exhibited much lower resistivities (≈30 mΩ cm). This feature was reported previously^[5] for CuI films made by solid iodination due to an excess of carrier density. The carrier density in our CuI films could be decreased by an inert gas postanneal as suggested by an observed increase of the resistivity^[5] to 68 mΩ cm. Resistivity values reported for CuI films deposited by other

Table 1. ToF-ERDA elemental composition analysis of ALD CuO and corresponding converted CuI thin films.

Sample	Film thickness [nm]	Elemental ratio	Element atom %
Si/CuO ^{a)}	144	O: Cu 1.03	H 0.9
			C 0.5
			N 0.3
			O 49.8
			Cu 48.5
Si/CuI	318	Cu: I 1.08	H 0.4
			C 0.3
			N 0.1
			O 0.9
			Cu 51.0
			I 47.3

^{a)}Film deposited at 120 °C with 4440 cycles.

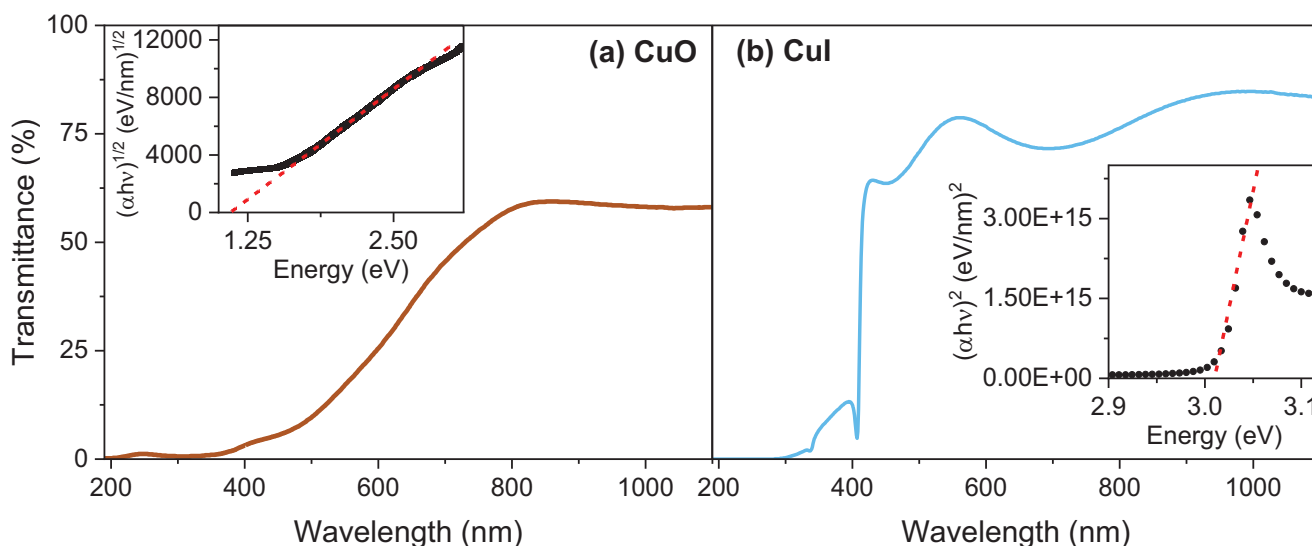


Figure 4. a) Transmittance spectra of a 75 nm CuO film on a sapphire substrate. Inset shows the Tauc plot of the CuO film. b) Transmittance spectra of the corresponding converted CuI film on a sapphire substrate. Inset shows the Tauc plot of the CuI film.

methods are 54 mΩ cm by sputtering,^[56] 100 mΩ cm by PLD,^[57] and 74 mΩ cm by thermal evaporation.^[58] Our CuI films were p-type, as determined by the hot-point probe technique.

To verify the easy and straightforward applicability of CuI thin films made by this route, we demonstrate the deposition of CuI on ALD n-type TiO₂^[59] to form a pn-junction as a proof-of-concept diode structure. After the conversion to CuI, we performed a post-anneal in N₂ atmosphere at 150 °C for 1 h to increase the resistivity of CuI according to literature.^[5] We measured the current-voltage (*I*-*V*) curve of a pn-junction made from 58 nm thick CuI on 73 nm thick TiO₂ (Figure 5b). The shape of the resulting curve is typical for a diode. Without any further process optimizations an ideality factor of $\eta = 4.4$ was determined for this diode structure (Figure S7, Supporting Information). Large ideality factor values > 2 were reported previously^[60,61] and indicate, e.g., series resistance, interface interdiffusion, or a strained interface.

To prove the compatibility of our process with a halide perovskite in PSC applications, we prepared a CuO film via ALD on γ -CsPbI₃ perovskite and subsequently converted it to CuI without affecting the perovskite. This was considered challenging since γ -CsPbI₃ can easily transform into its nonperovskite δ -CsPbI₃ phase upon exposure to oxygen and/or at elevated temperatures. For this reason, we chose the lowest possible deposition temperature for the ALD CuO process (80 °C). Furthermore, to decrease the exposure of the perovskite to the precursor pulses during the ALD CuO process, we decreased both pulse durations to 0.5 s for the first 100 cycles. The resulting CuO film was amorphous and the sample did not show any other reflections in the X-ray diffractogram than those of γ -CsPbI₃, thereby verifying that it was unaffected by the CuO deposition (Figure S8, Supporting Information). Even though it was not possible to characterize the CuO by grazing incidence XRD (GIXRD), we were able to indicate the CuO deposition

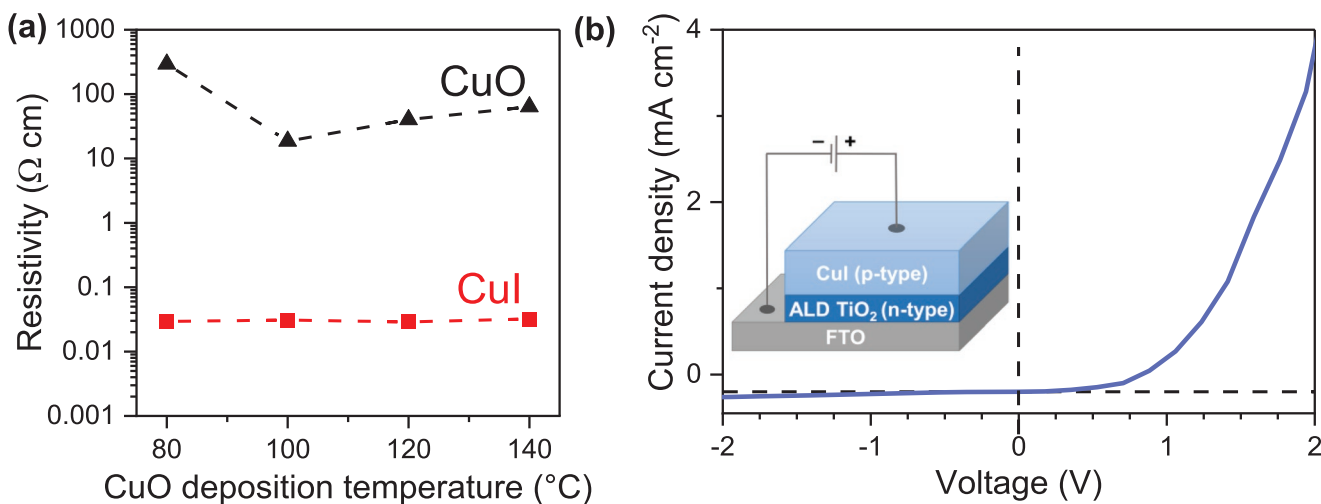


Figure 5. a) Resistivity as a function of the CuO deposition temperature for CuO and the corresponding converted CuI thin films. b) Current density as a function of applied voltage (*I*-*V*) from a CuI-TiO₂ pn-junction. Inset: Experiment setup scheme.

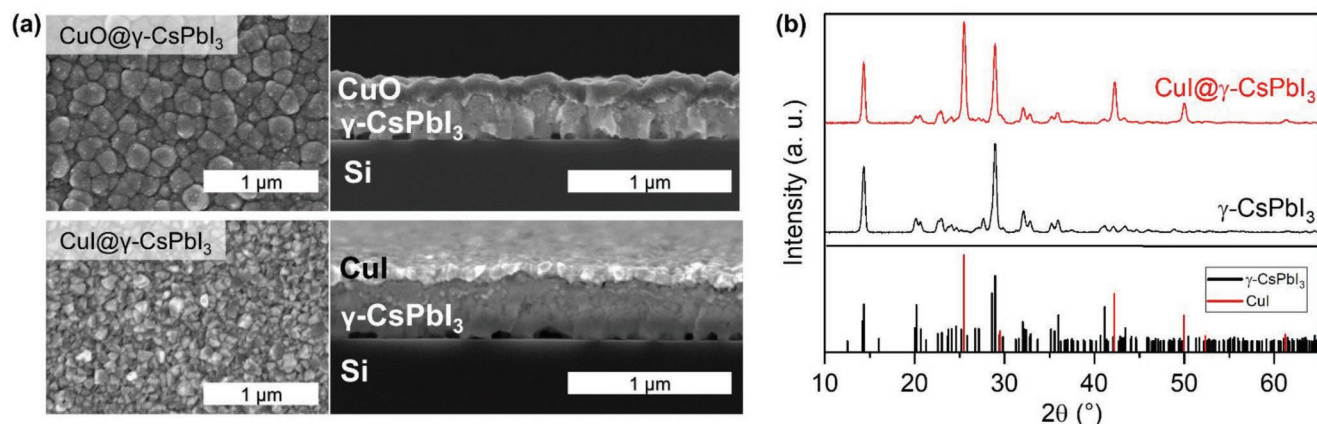


Figure 6. a) Top-down (left) and cross-sectional (right) SEM images after deposition of ALD CuO on γ -CsPbI₃ used as a substrate (top) and after conversion of CuO into CuI (bottom). b) Corresponding GIXRD patterns of initial γ -CsPbI₃ used as a substrate and after deposition CuI on top of it.

from EDS line scans (Figure S9, Supporting Information). The SEM images reveal that the CuO film uniformly encapsulates the γ -CsPbI₃ film without the appearance of pinholes (Figure 6a, top row). After converting the CuO to CuI, clear reflections in the X-ray diffractogram indicate the formation of CuI without affecting the underlying γ -CsPbI₃ (Figure 6b). SEM images support this conclusion by demonstrating a uniform and pinhole-free CuI film encapsulating the γ -CsPbI₃ film (Figure 6a, bottom row).

3. Conclusion

We described a new two-step approach for the deposition of transparent and conductive p-type CuI thin films. Our approach relies on ALD as a key method to enable conformal and scalable thin film deposition which is crucial for many applications, such as PSCs. We deposited CuO thin films by ALD and subsequently converted them by exposure to HI vapor at room temperature into phase-pure and uniform CuI thin films of high purity. The conversions were fast (5 min) and easily set up. Challenges occurred upon conversion of very thin or thick CuO films: thin initial films (< 25 nm) had pinholes after the conversion, whereas thick initial films (> 100 nm) tended to burst and peel off of the substrates during the conversion. Furthermore, we successfully demonstrated CuI deposition on several substrates, such as amorphous Al₂O₃, γ -CsPbI₃ perovskite and n-type TiO₂. The successful deposition of CuI on γ -CsPbI₃ proves the compatibility of our process for using CuI as the hole transport layer in perovskite solar cell applications in a nip-configuration. With the resulting n-TiO₂/p-CuI structure we fabricated a diode structure as a proof-of-concept device. We believe that the ALD-based approach described in this work will offer a viable alternative for depositing transparent p-type conductive CuI thin films in applications that involve complex high aspect ratio structures or large substrate areas.

4. Experimental Section

Film Deposition: CuO thin films were grown in a commercial cross-flow F-120 ALD reactor (ASM Microchemistry Ltd., Finland)

under reduced nitrogen pressure (99.999%, AGA, about 10 mbar) at different temperatures. Nitrogen was used as a carrier and purging gas and led into the reactor through a gas purifier (SAES Pure Gas, MCI-902F, H₂O, O₂, CO, CO₂, H₂, nonmethane hydrocarbon (NMHC) removal <1 ppb). Precursor pulsing was realized by inert gas valving. The CuO depositions were carried out using synthesized solid bis(dimethylamino-2-propoxy) copper(II) (Cu(dmap)₂) and ozone (O₃). Cu(dmap)₂ was synthesized following the procedure reported in literature^[62] and sublimed from an open quartz boat held inside the reactor at 65 °C. Ozone was produced from oxygen (Woikoski, 99.999%) using a Wedeco Ozomatic Modulator 4 HC Lab Ozone generator (ozone concentration of ≈ 100 g Nm⁻³) and introduced to the reactor using needle and solenoid valves.

Primarily native oxide covered 5 × 5 cm² silicon (100) (Si, Okmetic) was used as a substrate for the CuO depositions. Additionally, for some depositions sapphire wafers (2", University Wafer) were used as substrates. Sapphire wafers were heated at 1000 °C in an air oven for 2 h to induce atomic step formation.^[63,64] Prior to deposition, all substrates except sapphire were cleaned in an ultrasonic bath, first in a solution of industrial strength cleaning concentrate (Branson) for 20 min at 50 °C, then in H₂O for 10 min at RT, and then in isopropanol for 10 min at RT. Cleaned substrates were dried in an oven at 100 °C and blown with N₂.

Al₂O₃ and TiO₂ underlayers (5 nm) were deposited at 75 °C with a Picosun SUNALE R-150 ALD reactor using the Al(CH₃)₃-H₂O and TiCl₄-H₂O processes, respectively. In both processes pulse and purge durations were 0.1 and 25 s, respectively. TiO₂ for the pn-junction structure was deposited with a F-120 ALD reactor on fluorine-doped tin oxide (FTO) at 250 °C using the Ti(OCH₃)₄-H₂O process.^[59] Ti(OCH₃)₄ (95%, Sigma-Aldrich) was sublimated at 130 °C. Pulse and purge durations were 1.0 s.

The ALD CsPbI₃ underlayer (200 nm) was made with a F-120 ALD reactor on Si with a two-step process described earlier.^[49] First, CsI was deposited with an ALD process at 150 °C and subsequently the film was exposed to the PbI₂ ALD process at 100 °C resulting in the CsPbI₃. For the CsI ALD process the pulse durations were 1.5 and 0.5 s for Cs(btsa) and SnI₄, respectively, purge durations were 1.0 s, and 300 cycles were applied. For the PbI₂ ALD process, the pulse durations were 0.8 and 2 s for Pb(btsa)₂ and SnI₄, respectively, purge durations were 1.0 s, and 3000 cycles were applied on top of the CsI to convert it to CsPbI₃. ALD CuO was deposited on top of CsPbI₃ at 80 °C by first applying 100 cycles using 0.5 s pulse durations for both O₃ and Cu(dmap)₂ precursors and 2.0 s purge durations, and subsequently applying 1900 cycles using 2.0 s of both pulse and purge durations.

Conversion to CuI: Gas phase conversions were performed in a 100 mL Erlenmeyer glass flask reactor containing a glass boat filled with 200 μ L hydroiodic acid (Sigma-Aldrich, 55%, no stabilizer) and ALD CuO thin film samples on a titanium sample rack. Hydroiodic acid was fresh and

stored in a refrigerator, and a micropipette was used for the transfer into the quartz boat. Reactions were performed at room temperature for 5 min under reduced pressure (<1 mbar). In addition, some of the reactions used a cooling bath (MGW Lauda RM6, 50/50 ethylene glycol: water) to reduce the conversion temperature.

Film Characterization: Surface morphology of the films was examined with a Hitachi S-4800 field emission scanning electron microscope (FESEM). CuI film thicknesses were determined from energy-dispersive X-ray spectroscopy (EDS) data measured using an Oxford INCA 350 microanalysis system connected to the FESEM. The thicknesses were calculated from the EDS data with GMRFilm software^[65] using bulk density of CuI (5.67 g cm⁻³). The errors in thickness values were estimated using weight % uncertainty in the EDS measurements and the propagation of uncertainty expression. Element concentrations were estimated from EDS data using IL- α , and Cu K α lines.

GIXRD patterns were measured with a Rigaku Smartlab diffractometer using a Cu K α ($\lambda = 1.54 \text{ \AA}$) X-ray beam and parallel beam optics. For CuO and CuI films an incidence angle of 1° was used in the GIXRD measurements. CuO film thicknesses were determined from X-ray reflectivity (XRR) measurements.

Element contents in the films were evaluated with time-of-flight elastic recoil detection analysis (ToF-ERDA) with a 40° scattering angle with 20° beam-in and recoils-out geometry with respect to the target surface. The applied Br⁸⁺ beam energy was 40 MeV.

Optical measurements (UV–vis) were performed with a Hitachi U2000 spectrophotometer. Transmittance spectra measured from samples deposited on sapphire were used for the construction of Tauc plots from which the optical bandgaps were estimated.^[53,54] Based on literature, the bandgap of CuO was assumed to be indirect allowed, whereas the bandgap for CuI was assumed to be direct allowed.

Atomic force microscopy (AFM) was performed using a Veeco Multimode V instrument. Tapping mode images were captured in air using silicon probes with a nominal tip radius of 10 nm and a nominal spring constant of 3 N m⁻¹ (NTESP-75 from Bruker). Images were flattened to remove artefacts caused by a sample tilt and a scanner bow. Measurements were taken from 1 × 1 μm^2 sample areas. Roughness was calculated as root-mean-square (R_q) value.

Resistivity of the films deposited on soda-lime glass was measured with a 4-point-probe system (CPS Probe Station, Cascade Microtech) connected to a Keithley 2400 source meter. The same source meter was used for current-voltage (I – V) measurements of the pn-junction structures. In the I – V measurements, the contacts were made with needle probes to FTO and CuI. InGa eutectic ($\geq 99.99\%$, Sigma-Aldrich) was applied to the contact area.

The ideality factor was determined from the slope of a linear fit in the low voltage region of the $\ln|I|/V$ curve.

Supporting Information

Supporting Information is available from the Wiley Online Library or from the author.

Acknowledgements

The authors thank Academy of Finland (Decision No. 330086) and the Finnish Center of Excellence in Atomic Layer Deposition (ALDCoE 2012–2017) for financial support. The work was conducted in the ALD center, Finland, infrastructure.

Conflict of Interest

The authors declare no conflict of interest.

Data Availability Statement

The data that support the findings of this study are available from the corresponding author upon reasonable request.

Keywords

atomic layer deposition, copper(I) iodide, hole transport layer, perovskite solar cell, transparent p-type semiconductor

Received: August 24, 2022

Revised: October 14, 2022

Published online:

- [1] M. N. Amalina, Y. Azilawati, N. Rasheid, M. Rusop, *Proc. Eng.* **2013**, 56, 731.
- [2] M. Grundmann, F. L. Schein, M. Lorenz, T. Böntgen, J. Lenzner, H. von Wenckstern, *Phys. Status Solidi A* **2013**, 210, 1671.
- [3] A. Liu, H. Zhu, M. G. Kim, J. Kim, Y. Y. Noh, *Adv. Sci.* **2021**, 8, 2100546.
- [4] D. Chen, Y. Wang, Z. Lin, J. Huang, X. Chen, D. Pan, F. Huang, *Cryst. Growth Des.* **2010**, 10, 2057.
- [5] N. Yamada, R. Ino, Y. Ninomiya, *Chem. Mater.* **2016**, 28, 4971.
- [6] C. Yang, M. Kneiß, M. Lorenz, M. Grundmann, *Proc. Natl. Acad. Sci. USA* **2016**, 113, 12929.
- [7] V. Raj, T. Lu, M. Lockrey, R. Liu, F. Kremer, L. Li, Y. Liu, H. H. Tan, C. Jagadish, *ACS Appl. Mater. Interfaces* **2019**, 11, 24254.
- [8] C. Yang, D. Souchay, M. Kneiß, M. Bogner, H. Wei, M. Lorenz, O. Oeckler, G. Benstetter, Y. Q. Fu, M. Grundmann, *Nat. Commun.* **2017**, 8, 16076.
- [9] J. Coroa, B. M. Faustino, A. Marques, C. Bianchi, T. Koskinen, T. Juntunen, I. Tittonen, I. Ferreira, *RSC Adv.* **2019**, 9, 35384.
- [10] B. M. Morais Faustino, D. Gomes, J. Faria, T. Juntunen, G. Gaspar, C. Bianchi, A. Almeida, A. Marques, I. Tittonen, I. Ferreira, *Sci. Rep.* **2018**, 8, 6867.
- [11] F.-L. Schein, H. von Wenckstern, M. Grundmann, *Appl. Phys. Lett.* **2013**, 102, 092109.
- [12] A. Annadi, N. Zhang, D. Boon Kiang Lim, H. Gong, *ACS Appl. Mater. Interfaces* **2020**, 12, 6048.
- [13] J. H. Lee, W.-J. Lee, T. H. Kim, T. Lee, S. Hong, K. H. Kim, *J. Phys.: Condens. Matter* **2017**, 29, 384004.
- [14] K. Ding, Q. Hu, D. Chen, Q. Zheng, X. Xue, F. Huang, *IEEE Electron Device Lett.* **2012**, 33, 1750.
- [15] J.-H. Cha, D.-Y. Jung, *ACS Appl. Mater. Interfaces* **2017**, 9, 43807.
- [16] H. Zhu, A. Liu, Y.-Y. Noh, *IEEE Electron Device Lett.* **2020**, 41, 1033.
- [17] A. Annadi, N. Zhang, D. B. K. Lim, H. Gong, *ACS Appl. Electron. Mater.* **2019**, 1, 1029.
- [18] H. J. Lee, S. Lee, Y. Ji, K. G. Cho, K. S. Choi, C. Jeon, K. H. Lee, K. Hong, *ACS Appl. Mater. Interfaces* **2019**, 11, 40243.
- [19] S. Lee, H. J. Lee, Y. Ji, S. M. Choi, K. H. Lee, K. Hong, *J. Mater. Chem. C* **2020**, 8, 9608.
- [20] C.-H. Choi, J. Y. Gorecki, Z. Fang, M. Allen, S. Li, L.-Y. Lin, C.-C. Cheng, C.-H. Chang, *J. Mater. Chem. C* **2016**, 4, 10309.
- [21] B. Gil, A. J. Yun, Y. Lee, J. Kim, B. Lee, B. Park, *Electron. Mater. Lett.* **2019**, 15, 505.
- [22] L. C. Palilis, M. Vasilopoulou, A. Verykios, A. Soulati, E. Polydorou, P. Argitis, D. Davazoglou, A. R. b. Mohd Yusoff, M. K. Nazeeruddin, *Adv. Energy Mater.* **2020**, 10, 2000910.
- [23] Y. Wang, R. Wensch, R. Schlattmann, I. Lauermaun, *Adv. Energy Mater.* **2018**, 8, 1801692.

- [24] Z. Yu, L. Sun, *Small Methods* **2018**, *2*, 1700280.
- [25] J. T. Matondo, D. M. Maurice, Q. Chen, L. Bai, M. Guli, *Sol. Energy Mater. Sol. Cells* **2021**, *224*, 111011.
- [26] J.-P. Correa-Baena, M. Saliba, T. Buonassisi, M. Grätzel, A. Abate, W. Tress, A. Hagfeldt, *Science* **2017**, *358*, 739.
- [27] M. Jeong, I. W. Choi, E. M. Go, Y. Cho, M. Kim, B. Lee, S. Jeong, Y. Jo, H. W. Choi, J. Lee, *Science* **2020**, *369*, 1615.
- [28] M. Green, E. Dunlop, J. Hohl-Ebinger, M. Yoshita, N. Kopidakis, X. Hao, *Prog. Photovoltaics* **2021**, *29*, 3.
- [29] S. S. Mali, C. K. Hong, *Nanoscale* **2016**, *8*, 10528.
- [30] S. Sahare, H. D. Pham, D. Angmo, P. Ghoderao, J. MacLeod, S. B. Khan, S. L. Lee, S. P. Singh, P. Sonar, *Adv. Energy Mater.* **2021**, *11*, 2101085.
- [31] Y. Rong, Y. Hu, A. Mei, H. Tan, M. I. Saidaminov, S. I. Seok, M. D. McGehee, E. H. Sargent, H. Han, *Science* **2018**, *361*, eaat8235.
- [32] F. Wang, Y. Cao, C. Chen, Q. Chen, X. Wu, X. Li, T. Qin, W. Huang, *Adv. Funct. Mater.* **2018**, *28*, 1803753.
- [33] A. Rajagopal, K. Yao, A. K. Y. Jen, *Adv. Mater.* **2018**, *30*, 1800455.
- [34] F. Huang, M. Li, P. Siffalovic, G. Cao, J. Tian, *Energy Environ. Sci.* **2019**, *12*, 518.
- [35] Y. S. Kim, S. J. Yun, *Appl. Surf. Sci.* **2004**, *229*, 105.
- [36] F. Lee, S. Marcus, E. Shero, G. Wilk, J. Swerts, J. W. Maes, T. Blomberg, A. Delabie, M. Gros-jean, E. Deloffre, *2007 IEEE/SEMI Advanced Semiconductor Manufacturing Conference*, IEEE, New York **2007**, p. 359.
- [37] V. Miikkulainen, M. Leskelä, M. Ritala, R. L. Puurunen, *J. Appl. Phys.* **2013**, *113*, 2.
- [38] M. Ritala, M. Leskelä, in *Handbook of Thin Films*, Academic Press **2002**, pp. 103–159.
- [39] M. Leskelä, M. Ritala, *Angew. Chem., Int. Ed.* **2003**, *42*, 5548.
- [40] M. Knaut, M. Junige, V. Neumann, H. Wojcik, T. Henke, C. Hossbach, A. Hiess, M. Albert, J. W. Bartha, *Microelectron. Eng.* **2013**, *107*, 80.
- [41] K. Ali, K.-H. Choi, *Langmuir* **2014**, *30*, 14195.
- [42] L. Hoffmann, K. O. Brinkmann, J. Malerczyk, D. Rogalla, T. Becker, D. Theirich, I. Shutsko, P. Görrn, T. Riedl, *ACS Appl. Mater. Interfaces* **2018**, *10*, 6006.
- [43] B. O'Donnell, Atomic Layer Deposition Storms Market for PERC, PV Magazine International, *6*, June **2019**, <https://www.pv-magazine.com/2019/06/29/the-weekend-read-atomic-layer-deposition-storms-market-for-perc/> (accessed: 14 Oct 2022).
- [44] A. N. Fioretti, M. Morales-Masis, *J. Photonics Energy* **2020**, *10*, 042002.
- [45] J. Willis, D. O. Scanlon, *J. Mater. Chem. C* **2021**, *9*, 11995.
- [46] Database of Materials Prepared by Atomic Layer Deposition (ALD), **2022**, <https://www.atomiclimits.com/alddbatabase/> (accessed: October 2022).
- [47] G. Popov, M. Mattinen, T. Hatanpää, M. Vehkamäki, M. Kemell, K. Mizohata, J. Räisänen, M. Ritala, M. Leskelä, *Chem. Mater.* **2019**, *31*, 1101.
- [48] J. N. Vagott, K. Bairley, J. Hidalgo, C. A. Perini, A.-F. Castro-Méndez, S. Lombardo, B. Lai, L. Zhang, K. Kisslinger, J. Kacher, *Chem. Mater.* **2022**, *34*, 2553.
- [49] A. Weiß, G. Popov, E. Atosuo, A. Vihervaara, P. Jalkanen, M. Vehkamäki, M. Leskelä, M. Ritala, M. Kemell, *Chem. Mater.* **2022**, *49*, 6087.
- [50] G. Popov, M. Mattinen, M. L. Kemell, M. Ritala, M. Leskelä, *ACS Omega* **2016**, *1*, 1296.
- [51] T. Iivonen, J. Hämäläinen, B. Marchand, K. Mizohata, M. Mattinen, G. Popov, J. Kim, R. A. Fischer, M. Leskelä, *J. Vac. Sci. Technol., A* **2016**, *34*, 01A109.
- [52] S. Åsbrink, L.-J. Norrby, *Acta Crystallogr., Sect. B: Struct. Crystallogr. Cryst. Chem.* **1970**, *26*, 8.
- [53] R. Swanepoel, *J. Phys. E: Sci. Instrum.* **1983**, *16*, 1214.
- [54] M. Sreemany, S. Sen, *Mater. Chem. Phys.* **2004**, *83*, 169.
- [55] A. Tripathi, T. Dixit, J. Agrawal, V. Singh, *Appl. Phys. Lett.* **2020**, *116*, 111102.
- [56] T. Tanaka, K. Kawabata, M. Hirose, *Thin Solid Films* **1996**, *281*, 179.
- [57] B. Zhu, X. Zhao, *Phys. Status Solidi A* **2011**, *208*, 91.
- [58] M. Zi, J. Li, Z. Zhang, X. Wang, J. Han, X. Yang, Z. Qiu, H. Gong, Z. Ji, B. Cao, *Phys. Status Solidi A* **2015**, *212*, 1466.
- [59] V. Pore, A. Rahtu, M. Leskelä, M. Ritala, T. Sajavaara, J. Keinonen, *Chem. Vap. Deposition* **2004**, *10*, 143.
- [60] X. Li, L. Liang, H. Cao, R. Qin, H. Zhang, J. Gao, F. Zhuge, *Appl. Phys. Lett.* **2015**, *106*, 132102.
- [61] A. Tataroğlu, A. G. Al-Sehemi, M. Ilhan, A. A. Al-Ghamdi, F. Yakuphanoglu, *Silicon* **2018**, *10*, 913.
- [62] R. Becker, A. Devi, J. Weiß, U. Weckenmann, M. Winter, C. Kiener, H. W. Becker, R. A. Fischer, *Chem. Vap. Deposition* **2003**, *9*, 149.
- [63] M. Yoshimoto, T. Maeda, T. Ohnishi, H. Koinuma, O. Ishiyama, M. Shinohara, M. Kubo, R. Miura, A. Miyamoto, *Appl. Phys. Lett.* **1995**, *67*, 2615.
- [64] H. Kim, D. Ovchinnikov, D. Deiana, D. Unuchek, A. Kis, *Nano Lett.* **2017**, *17*, 5056.
- [65] R. Waldo, *Microbeam Analysis*, San Francisco Press, San Francisco, CA **1988**, p. 310.